ACADEMIA ROMÂNĂ
Revue Roumaine de Chimie
https://web.icf.ro/rrch/

Rev. Roum. Chim.,
2022, *67*(10–12), 579–589
DOI: 10.33224/rrch.2022.67.10-12.07

SYNTHESIS AND CYTOTOXIC ACTIVITY EVALUATION OF 1,4-DIHYDROPYRIDINE DERIVATIVES USING $Ag_2O/GO/TiO_2$ COMPOSITE NANOSTRUCTURE

Fatemeh Samandi ZADEH,[a] Mohammad Kazem MOHAMMADI, [b,*] Ayeh RAYATZADEH[a] and Neda HASANZADEH[a]

[a]Department of Chemistry, Ahvaz Branch, Islamic Azad University, Ahvaz, Iran
[b]Advanced Surface Engineering and Nano Materials Research Center, Department of Chemistry, Ahvaz Branch, Islamic Azad University, Ahvaz, Iran

Received September 19, 2022

$Ag_2O/GO/TiO_2$ composite nanostructure was established as a heterogeneous catalyst for the one pot synthesis of dihydropyridine derivatives via Hantzsch reaction. The synthetic method was mainly used in the presence of $Ag_2O/GO/TiO_2$ nano composite as a heterogeneous solid catalyst. This nano composite catalyzed Hantzsch reaction afforded good yields (87–95%) in solvent free condition at 90 °C. A broad range of structurally diverse aldehydes were applied successfully, and corresponding products were obtained in high yields without any byproduct. Compared with other methods, satisfactory results are obtained with high yields, short reaction times, and simplicity in the experimental procedure. Cytotoxic activities for some of the synthesized compounds were evaluated by MTT assay in three human cancer cell lines (HeLa, LS180 and Raji). Half of the tested compounds showed good cytotoxicity in Raji cells. Diethyl 4-(2,4-dichlorophenyl)-1,4-dihydro-2,6-dimethylpyridine-3,5-dicarboxylate (3 i) was found to be the most potent molecule among the studied 1, 4 dihydropyridines derivatives. Electron withdrawing groups along with heterocyclic rings bearing more hetero atoms seemed to be necessary factors in providing higher cytotoxic activities in Raji cell lines.

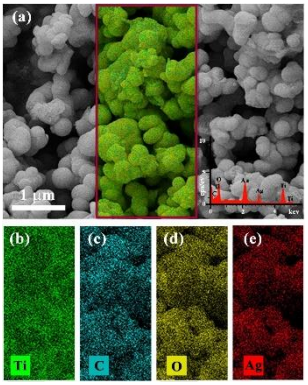

INTRODUCTION

Graphene oxide (GO), consisting of two carbon sheets with closed lattice structure, has gathered widespread interest as a catalyst and catalytic support due to presence of surface bound active functional sites, large surface area, and excellent thermal and mechanical properties.[1] Primary cause for high activity of GO is the presence of hydroxyl, carboxylic and epoxy groups which shows high acidity, excellent oxidizing properties, good conductivity, etc.[2-4] Organic transformations are catalyzed by graphene oxide utilizing its acidic protons or its strong oxidizing ability showing potential to replace the traditional metal catalyzed pathways. Numerous one pot syntheses such as a-aminophosphonate synthesis, benzimidazole synthesis, epoxidation, Michael addition, aldol condensation etc., are accelerated by surface bound hydroxyl and carboxylic acid groups in GO.[5-9] Catalytic activity of graphene oxide refers to presence of functional groups. Further, the

* Corresponding author: mkmohamadi@gmail.com

properties of graphene can be amazing by incorporating other functional groups on the GO sheets. It was found that synthesis method could impact the properties of graphene oxide.[10-12]

With the development of nanotechnology, catalysts made of transition metals have drawn a lot of attention due to their application in various areas including organic transformations, rechargeable batteries, and wastewater treatment.[13] Transition metals (Co, Fe, Ni, Mo, Mn, and Zn, etc.) show advantages such as being inexpensive, non-toxic, and abundant in the earth.[14] The applications of N^O (ethyl imino-methyl) phenol Fe(II) and Co(II) complexes in ethylene oligomerization catalysis and their structural elucidation were studied by Ngcobo *et al.*[15] In artificial photosynthetic systems, hydrogen is generated with molecular catalysts of Co, Ni, Fe, and Mo[16] carried out theoretical and experimental studies on metal-organic frame derived (M=Fe, Ni, Zn, and Mo) which were doped into Co_9S_8 nano arrays as an efficient electro catalyst for water splitting.[14]

Recently, noticeable growth has been observed in the applications of heterogeneous catalysis in organic reactions to carry out synthetic transformations as a result of its significance in terms of enviro-economical and practical aspects.[17]

Reportedly, in MCRs a wide range of catalysts has been explored in the synthesis of 1,4-DHP derivatives including L-proline,[18,19] aspartic acid,[20] p-toluenesulfonic acid monohydrate,[21-23] TiO_2 nano wires,[24] phosphootungstic acid ($H_3PW_{12}O_{40}$),[25] silica-coated nano-Fe_3O_4,[26] cellulose sulfuric acid,[27] chitosan supported copper(II)sulfate (CSCS),[28] porcine pancreatic lipase,[29] Magnetic dextrin nano biomaterial,[30] SO_3H-functionalized nano-MGO-D-NH_2,[31] guanidinylated chitosan magnetic nano catalyst,[32] and pyrimidine-2,4-diamine (PDA)-functionalized silica-coated magnetic nanocatalyst (Fe_3O_4/SiO_2-PDA)[33] and ceric ammonium nitrate (CAN).[34]

1,4-dihydropyridines were first synthesized by Arthur Hantzch in 1882. Dihydropyridines have various and important uses, including 1,4-dihydropyridines, in the four positions of which quinoline is extracted, which is used as a painkiller. Morphine is known as one of the most popular 1,4-dihydropyridines, which is used as an antihypertensive drug. Another role of 1,4-dihydropyridines is their function as an antihypertensive drug by dilating the walls of blood vessels.

Nevertheless, most protocols for the synthesis of these compounds have severe limitations, for example, low yields, high cost and catalyst loadings, and low catalyst recovery and recyclability. In continuation of our interest in the synthesis of new nanostructure compounds,[35,36] herein, we report the preparation of $Ag_2O/GO/TiO_2$ structures on graphene materials and the catalytic activity of this new zeolite nano catalyst evaluated for the synthesis of a wide range of 1,4-dihydropyridine derivatives with high structural diversity through the reaction protocols. Furthermore, the cytotoxic activity of synthesized compound was checked in five different cell lines.

EXPERIMENTAL

Materials

Reagents like ethylacetoaceat, ammonium acetat, titanium dioxide (TiO_2), ammonium heptamolybdate tetrahydrate $(NH_4)_6Mo_7O_{24}\cdot 4H_2O$, and aromatic aldehydes were purchased from Merck company and used without any purifications. Distilled water was used for these synthesis methods.

Cytotoxicity assay materials and conditions

RPMI 1640, fetal bovine serum (FBS), trypsin and phosphate buffered saline (PBS) were purchased from Biosera (Ringmer, UK). 3-(4, 5-dimethylthiazol-2-yl)-2,5-diphenyltetrazolium bromide (MTT) was obtained from Sigma (Saint Louis, MO, USA) and penicillin/streptomycin was purchased from Invitrogen (San Diego, CA, USA). Doxorubicin and dimethyl sulphoxide were obtained from EBEWE Pharma (Unterach, Austria) and Merck (Darmstadt, Germany), respectively. HeLa (human cervical adenocarcinoma), LS-180 (human colon adenocarcinoma), and Raji (human B lymphoma) cells were obtained from the National Cell Bank of Iran, Pasteur Institute, Tehran, Iran. All cell lines were maintained in RPMI 1640 supplemented with 10% FBS, and 100 units/mL penicillin-G and 100 µg/mL streptomycin. Cells were grown in monolayer cultures, except for Raji cells, which were grown in suspension, at 37 °C in humidified air containing 5% CO_2.

Cell viability following exposure to synthetic compounds was estimated by using the MTT reduction assay.[37] HeLa, LS-180, and Raji cells were plated in 96-well flat-bottomed microplates at densities of 25,000, 100,000, and 50,000 cells/mL, respectively (100 µL per well). Control wells contained no drugs and blank wells contained only growth medium for background correction. After overnight incubation at 37°C, half of the growth medium was removed and 50 µL of medium supplemented with different concentrations of synthetic compounds dissolved in DMSO were added in quadruplicate. Plates with Raji cells were centrifuged before

this procedure. Maximum concentration of DMSO in the wells was 0.5%. Cells were further incubated for 72 h, except for HeLa cells, which were incubated for 96 h. At the end of the incubation time, the medium was removed and MTT was added to each well at a final concentration of 0.5 mg/mL and plates were incubated for another 4 h at 37°C. Then, formazan crystals were solubilized in 200 µL DMSO. The turbidity was measured at 570 nm with background correction at 655 nm using a Bio-Rad micro plate reader (Model 680). The percentage of viability compared to control wells was calculated for each concentration of the compound and IC_{16} and IC_{50} values were calculated with the software Curve Expert version 1.34 for Windows. Each experiment was repeated 3–4 times. Data are presented as mean ± SD.

Instrumental techniques

The crystalline phase of the as-synthesized sample was identified by X-ray diffraction (XRD) measurements by the means of Ultime IV Multipurpose X-ray diffractometer equipped with Cu K () radiation. Fourier transform infrared (FT-IR) spectrum was obtained using Perkin Elmer BX-II spectrophotometer. Surface morphology was determined from field emission scanning electron microscopy (FESEM, Zeiss SIGMA VP-500) equipped with side detectors including energy-dispersive X-ray spectroscopy (EDS) and high-resolution elemental mapping to examine elemental compositions. The morphological features of the sample were investigated with a Zeiss (EM10C-Germany) transmission electron microscope (TEM) operating at 100 kV. All yields refer to the isolated products. Products were characterized by comparing their physical data, such as IR, ^{1}H NMR and ^{13}C NMR spectra with authentic samples. Using TMS as internal standard, NMR spectra were recorded in $CDCl_3$ on a Bruker Advance DPX 250 MHz spectrometer. Determination of the products' purity in the course of the reaction were monitored by TLC on silica gel poly gram SILG/UV 254 plates. Mass spectra were recorded on the MS model 5973 Network apparatus at ionization potential of 70 eV.

Synthesis of Ag_2O nanoparticles

In a typical synthesis process, 80 mL of a 0.005 M silver nitrate ($AgNO_3$) aqueous solution was heated at 60°C. After that, 20 mL of a 0.025 M sodium hydroxide aqueous solution was added drop by drop to the prepared $AgNO_3$ solution under continuous magnetic stirring at 60 ˚C for 2 h. After cooling down to the room temperature, the formed precipitate was collected by a centrifuge with a speed of 3000 rpm, washed with ethanol several times, and dried at a constant temperature of 40°C at 24 h.

Synthesis of $Ag_2O/GO/TiO_2$ composite nanoparticles

$Ag_2O/GO/TiO_2$ composite nanoparticles were synthesized through the sol-gel method according to the process reported by Xiao *et al.*[38] as follows: Firstly, 5 *g* of cetyltrimethylammonium bromide (CTAB) as the precursor of TiO_2 was added to 30 mL of ethanol and kept under continuous stirring. Secondly, 25 mL of a butyl titanate solution was separately dissolved in 50 mL of absolute ethanol and added to the obtained CTAB solution at the rate of one drop every 3 s. Thirdly, a solution containing 7 mg of as-synthesized Ag_2O nanoparticles in 5 mL of absolute ethanol, and another solution containing 20 mg of as-purchased graphene oxide in 10 mL of ethanol were prepared and slowly added to the above solution after 1 h. The resultant mixture was stirred for 2 h to reach a titanium dioxide gel. The obtained product was finally dried at 65 ˚C for 12 h and calcined at 450 ˚C for 2 h.

Typical procedure for the preparation of 1,4-dihydropyridine derivatives (4a-4g)

A mixture of ethyl acetate (0.26 g, 2 mmol), ammonium acetate (0.154 g, 2 mmol), aryl aldehyde (1 mmol) in the presence of graphene oxide nanocomposite (0.02 g) in a test tube at 90 °C in Conditions without solvent and placed in an oil bath. The progress of the reaction was assessed by TLC. After completion of the reaction observed by TLC, hot ethanol was added to the reaction mixture and the catalyst was separated by filter paper. The product was then crystallized with ethanol and water with a yield of 87 to 97%.

All products was characterized by comparison of melting points of synthesized compounds with reported literatures. (3a–j) (Scheme 1).

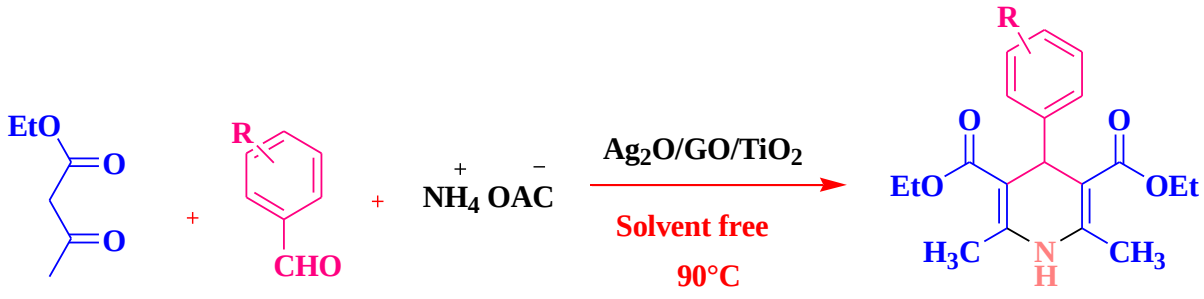

1 **2 a-j** **3 a-j**

Scheme 1 – Synthesis route for 1,4-dihydropyridine derivatives.

Table 1

Synthesis of 1, 4-dihydropyridine derivatives catalyzed by $Ag_2O/GO/TiO_2$ in solvent free condition

Entry	aldehyde	product	yield (%)	time (min)	m.p ˚C	m.p (ref)
1 3a	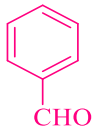	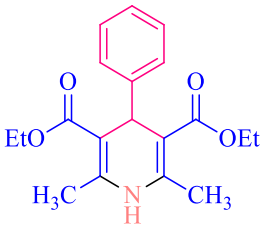	95	15	**158-159**	**158-160**
2 3b	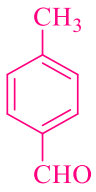	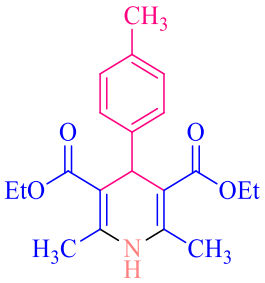	95	22	**136-138**	**135-137**
3 3c	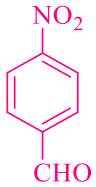	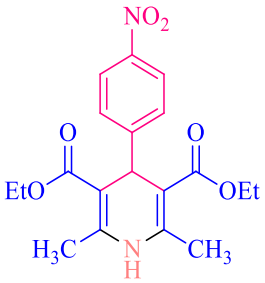	95	20	**128-130**	**130-132**
4 3d	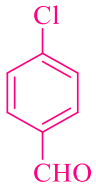	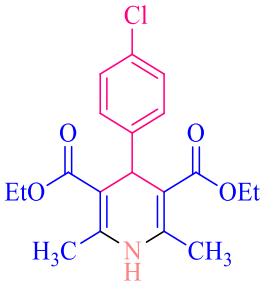	97	10	**144-145**	**144-145**
5 3e	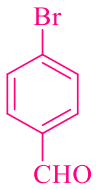	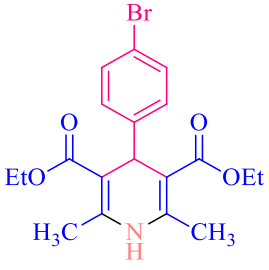	95	13	**162-163**	**160-162**

6 3f	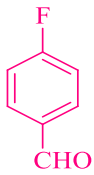	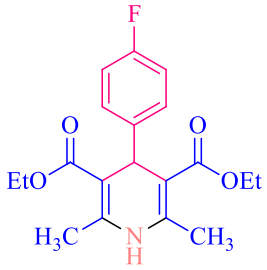	92	20	**155-157**	**153-156**
7 3g	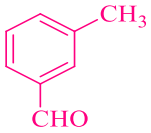	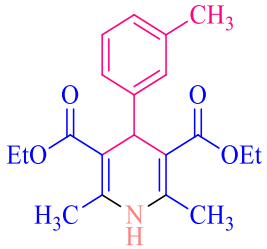	92	15	**122-125**	**122-124**
8 3h	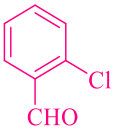	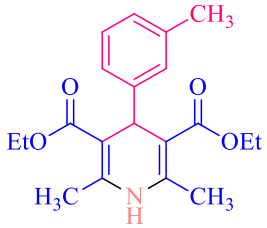	90	14	**214-216**	**216-218**
9 3i	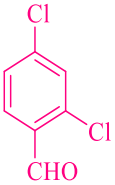	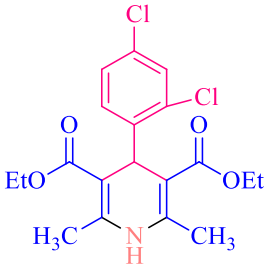	90	10	**108-109**	**108-110**
10 3j	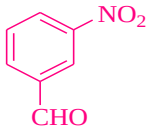	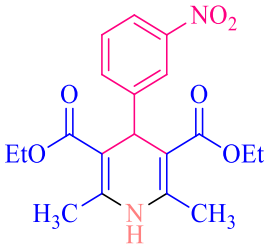	87	15	**165-167**	**166-168**

RESULTS AND DISCUSSION

$Ag_2O/GO/TiO_2$ composite

Phase compositions of as-synthesized nanoparticles were identified using the X-ray diffraction (XRD) technique. Fig. 1 displays the XRD pattern of $Ag_2O/GO/TiO_2$ composite nanoparticles. The XRD pattern of the composite nanoparticles exhibits four distinct peaks at 25.76°, 48.49°, 54.39°, and 55.53° corresponding to (101), (200), (105), and (211) crystal planes of anatase TiO_2 crystalline structure, respectively (JCPDS No. 00-021-1272). Two diffraction peaks are also found at 62.98° and 69.29°, which can be assigned to (214) and (301) planes of the TiO_2 rutile phase, respectively (JCPDS card No. 00-021-1276). The formation of Ag_2O structures is confirmed by arising characteristic peaks at 38.30°, 70.76°, and 75.55° relevant to (200), (222), and (311) Bragg planes, respectively (JCPDS No. 01-072-2108). As shown in Fig. 1, the presence of graphene sheets is justified by appearing a characteristic peak at

13.45° that can be indexed to carbon structures as presented in JCPDS card No. 01-089-8491. It is well known that the existence of GO in semiconductor composite structures compared to other carbon materials can improve the transitional performance of charge carriers relevant to high-temperature thermal effects.[33]

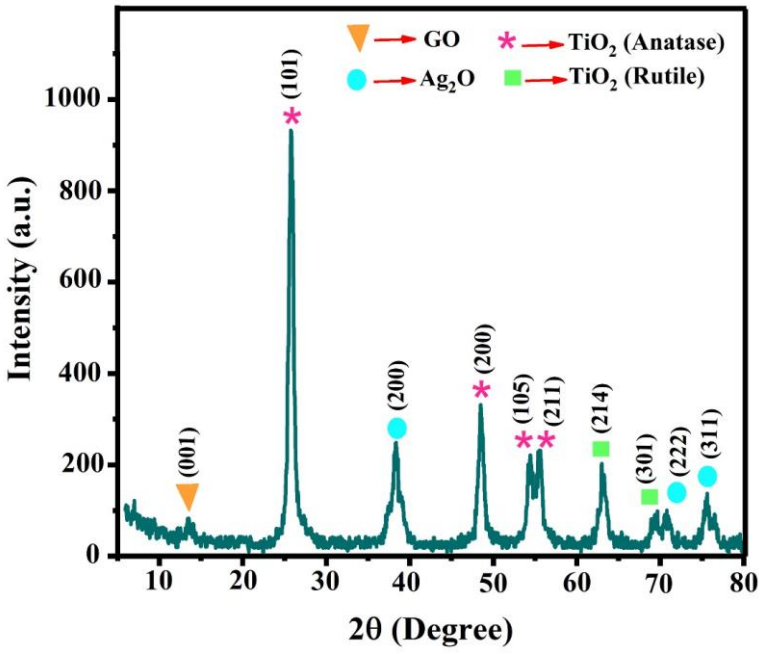

Fig. 1 – XRD pattern of $Ag_2O/GO/TiO_2$ composite nanoparticles.

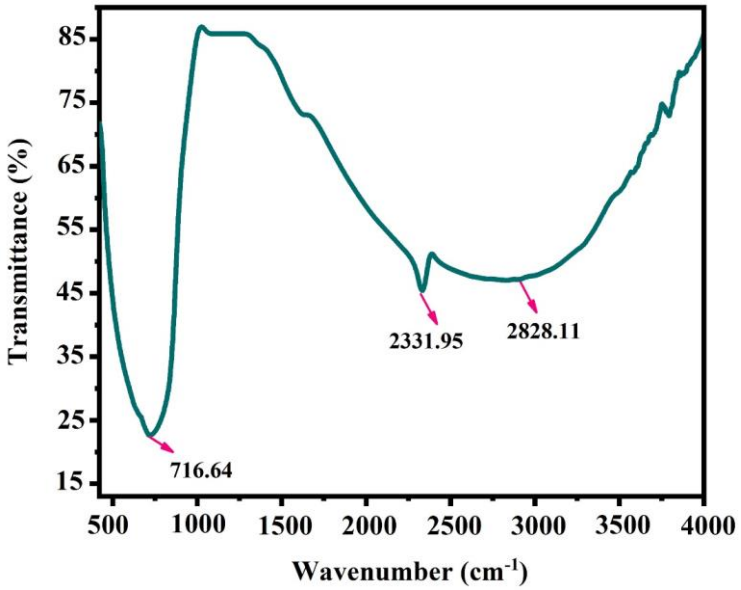

Fig. 2 – FTIR pattern of $Ag_2O/GO/TiO_2$ composite nanoparticles.

The surface chemical composition of the as-synthesized sample was investigated by FT-IR spectroscopy. Fig. 2 shows the FT-IR pattern of $Ag_2O/GO/TiO_2$ composite nanoparticles in the range of 450-4000 cm^{-1}. It can be seen in Fig. 2 that, due to Ti-O stretching in TiO_2 lattice, the absorption band appears at 716.64 cm^{-1}.[34] The characteristic band at 2331.95 cm^{-1} is ascribed to the stretching modes of carboxyl (C=O) groups.[14] The band observed at 2,828.11 cm^{-1} also corresponds to the C-H stretching frequency.[34]

The surface morphology of the as-synthesized sample was observed using FESEM micrographs. FESEM images of $Ag_2O/GO/TiO_2$ composite

nanoparticles in two different magnifications along with the corresponding histograms of particle size have been illustrated in Fig. 3. The FESEM image shown in Fig. 3a indicates a relatively uniform distribution from spherical-like particles with an average diameter of about 300 nm (Fig. 3c). It can be seen in Fig. 3b that the obtained spherical structures consist of numerous small nanoparticles with an average size of about 35 nm (Fig. 3d). Such a formed architecture revealed more available surface areas compared to that with simple spherical structures resulting in more improved performances for potential applications such as photocatalysis.

FESEM-EDS mapping was carried out to verify the surface element dispersion states of the as-synthesized sample. Fig. 4 presents the results obtained from the FESEM-EDS mapping of $Ag_2O/GO/TiO_2$ composite nanoparticles. Fig. 4b–e demonstrates the presence and uniform distribution of Ti, O, C, and Ag elements in the selected surface area of the as-synthesized sample (Fig. 4a), offering visual evidence for the successful formation of $Ag_2O/GO/TiO_2$ composite nanoparticles. EDS spectrum recorded for $Ag_2O/GO/TiO_2$ sample is also plotted as an inset in Fig. 4a indicating the existence of Ti, O, C, and Ag with atom percentages of 50.3%, 23.1%, 6.3%, and 20.3% in $Ag_2O/GO/TiO_2$ composite structure, respectively.

The morphological features of the sample were investigated with a Zeiss (EM10C-Germany) transmission electron microscope (TEM) operating at 100 kV. These images were prepared as follows: The dilute aqueous solution of the sample was sonicated for 15 min. Then, a portion of the sample (20 μL) was dropped onto holey carbon film on copper grid 300 mesh (EMS-USA) and dried thoroughly at room temperature.

For the closer look of synthesized microstructures, used of the transmission electron microscope (TEM). Transmission electron microscope image of $Ag_2O/GO/TiO_2$ showed in Fig. 5. TEM image of $Ag_2O/GO/TiO_2$ to be observed with the 50 nm to 300 nm magnification. According to figures, it can be said that the particles have irregular geometric shapes.

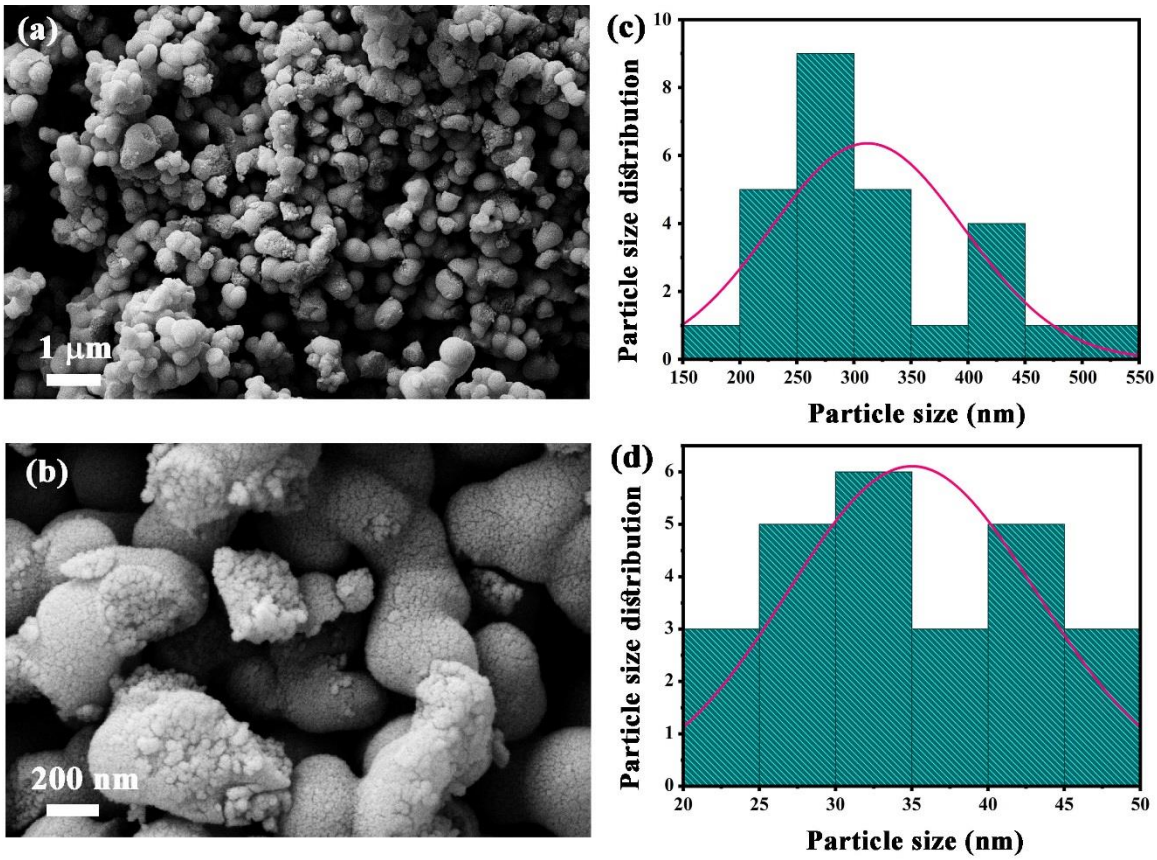

Fig. 3 – (a, b). Typical FESEM images and (c, d) the corresponding histograms of particle size for $Ag_2O/GO/TiO_2$ composite nanoparticles.

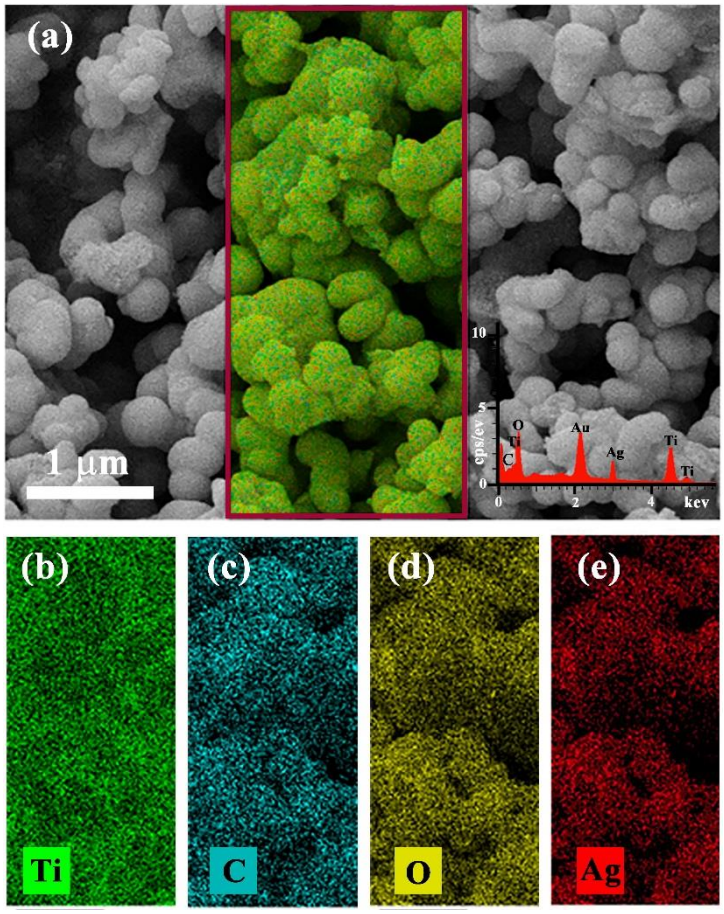

Fig. 4 – (a) FESEM image; Inset: corresponding EDS spectrum,
and (b-e) EDS mappings of $Ag_2O/GO/TiO_2$ composite nanoparticles.

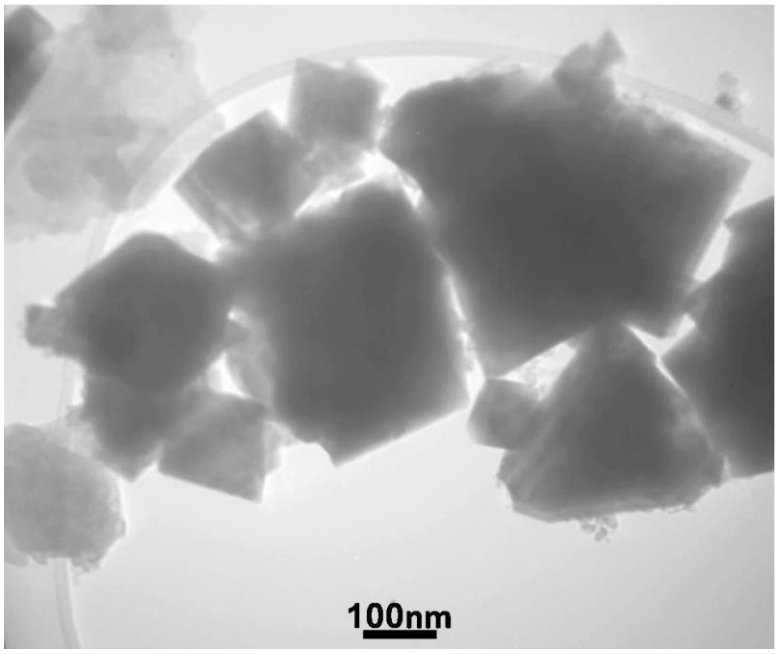

Fig. 5 – TEM image of $Ag_2O/GO/TiO_2$ composite nanoparticles.

Table 2

Hantzsch synthesis of diethyl 4-phenyl-2,6-dimethyl-1,4-dihydropyridine-3,5-dicarboxylate using ammonium acetate as nitrogen source: $Ag_2O/GO/TiO_2$ Composite compared with other methods

Entry	Conditions	Time (h:min)	Yield (%)
1	H_2SO_4	00:35	80
2	SiO_2	00:55	75
3	$PhB(OH)_2$	4:00	90
4	Silica gel/$NaHSO_4$	6:00	85
5	Ph_3P	5:00	72
6	Sulphonic acid on silica gel	5:30	90
7	Neat	1:30	93

To study the scope of the reaction, a series of aromatic aldehydes were investigated. The results are shown in Tables 1. In all cases, aromatic aldehydes substituted with either electron-donating or electron-withdrawing groups underwent the reaction smoothly and gave the products in excellent yields.

The role of $Ag_2O/GO/TiO_2$ in the reaction was the creation of wide substrate for the reaction of primary materials close to each other that help them to react efficiently. Moreover, metal oxides (Ag_2O and TiO_2) activated the carbonyl groups in the 1,3-dicarbonyl compounds that increase their reactivity with NH_2 groups. In Table 3, the comparison between the applications of this catalyst in synthesis of Bis dihydropyrimidones with other nano metal catalysts is depicted.

Comparison between the time and yield formation of diethyl 4-phenyl-2,6-dimethyl-1,4-dihydropyridine-3,5-dicarboxylate (3 b) using ammonium acetate as nitrogen source, ethyl acetoacetate and *p*-methyl aldehyde with other methods is listed in Table 2.

In order to carry out the synthesis of 1,4-dihydropyridine under environmentally benign conditions, Initially, the synthesis of 2,6-dimethyl4-phenyl-1,4-dihydro-pyridine-3,5-dicarboxylic acid diethyl ester was selected as a model reaction to optimize the reaction conditions. The reaction was carried out by heating a mixture of benzaldehyde (1 mmol), ethyl acetoacetate (2 mmol) and ammonium acetate (2 mmol) in the presence of various amount of $Ag_2O/GO/TiO_2$ composite nanostructure at different temperatures under solvent free conditions. The shortest time and best yield were achieved in the presence of 0.02 gr of catalyst at 90 °C. In order to elucidate the role of the $Ag_2O/GO/TiO_2$ composite nanostructure as catalyst, a control reaction was set up using benzaldehyde (1 mmol), ethyl acetoacetate (2 mmol) and ammonium acetate (2 mmol) in the absence of catalyst. The control reaction ended up with the formation of 10% of corresponding Hantzsch ester. However the test reaction set up with the same substrate, using 0.02 g of $Ag_2O/GO/TiO_2$ composite nanostructure at 90 °C under solvent free conditions afforded the product in 95% yield in 15 min.

In order to establish the true effectiveness of the nanostructure of catalyst, the condensation reaction was also tested using $Ag_2O/GO/TiO_2$ composite nanostructure under the same reaction condition. It clearly shows that although the reaction proceeded in the presence of $Ag_2O/GO/TiO_2$ composite (45%, 75 min), the best result was obtained in the presence of $Ag_2O/GO/TiO_2$ composite nanostructure. This may be due to considerable ratio of surface to volume in nanoparticles.

Cytotoxic effect on cancer cell lines

The half-maximal inhibitory concentration (IC_{50}) and (IC_{16}) are the most widely used and informative measure of a drug's efficacy. They indicate how much drug is needed to inhibit a biological process by 50 and 16 percentage, thus providing a measure of potency of an antagonist drug in pharmacological research. Most approaches to determine IC_{50} and IC_{16} of a pharmacological compound are based on assays that utilize whole cell systems.

The *in vitro* cytotoxic activities for 10 1,4-dihydropyridine derivatives are shown in Table 2. All the compounds under study showed superior cytotoxic activity on the Raji cells. Scheme 2 (Entry 9 –Table 2) showed higher cytotoxicity in all of the tested cells. This indicated that chlore as an electron withdrawing acceptor groups is a favorable structure for designing cytotoxic agents. This pathway may also be seen for other similar compounds (entry 4-6 – table 2) for Raji cell line. These compounds possess electron withdrawing halogen atoms (F,Cl,Br) on their aryl rings. It seems that halogen atoms can have an appropriate interaction with Raji cell receptors.

Table 3

Cytotoxic activity of some 1,4-dihydropyridine derivatives

Compound	HeLa cells		LS-180 cells		Raji cells	
	IC_{16} (µM)	IC_{50} (µM)	IC_{16} (µM)	IC_{50} (µM)	IC_{16} (µM)	IC_{50} (µM)
3 a	56±10.12	> 100	> 100	> 100	17.51 ±4.91	> 100
3 b	15.65 ±5.12	> 100	22.34±6.74	> 100	20.2 ±3.22	> 100
3 c	18.5 ±7.8	> 100	> 100	> 100	37.7 ±2.2	> 100
3 d	8.1 ±1,5	85.1 ±34.53	12.32 ±1.74	> 100	19.2 ±18.32	> 100
3 e	21.5 ±6.54	> 100	54.32 ±15.65	> 100	23.51 ±12.8	> 100
3 f	31.7 ±6.7	> 100	> 100	> 100	20.72 ±13.43	> 100
3 g	27.2 ±7.3	> 100	25.12±4.34	> 100	> 100	> 100
3 h	6.7 ±2.76	> 100	> 100	> 100	73.5 ±35	> 100
3 i	57 ±29.15	> 100	> 100	> 100	14.16 ±5.11	> 100
3 j	54.4 ±12.8	> 100	> 100	> 100	50.6 ±8.85	> 100
DOX	62.7 ±17.45	> 100	6.5 ±6	86.6 ±31.6	64 ±6.5	> 100
Cisplatin	2.3 ±0.65	8.6 ±2.1	6.6 ±1.95	35.8 ±13.1	2.7 ±0.3	11.3 ±1.25

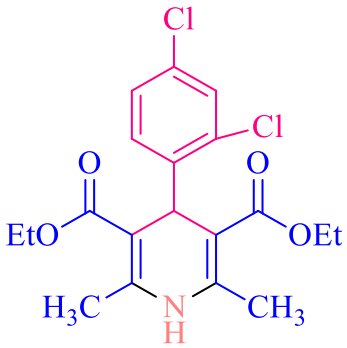

Scheme 2 – Diethyl 4-(2,4-dichlorophenyl)-1,4-dihydro-2,6-dimethylpyridine-3,5-dicarboxylate.

CONCLUSION

In conclusion, we successfully developed a simple and efficient method for preparation of a variety of 1,4-dihydropyridines by the one pot three-component reactions of different aromatic, hetero aromatic aldehydes, *β*-keto compounds and ammonium acetate in the presence comparing the performance of the present work with of a catalytic amount of $Ag_2O/GO/TiO_2$ composite nanostructure under solvent free conditions. 1, 4-dihydropyridine derivatives bearing heterocyclic substituents were synthesized and identified by comparing with instrumental analyses and reported literatures. All the tested compounds showed higher cytotoxic effect on Raji cancer cell lines compared to LS180 and Hela cancer cells. Electron withdrawing groups along with heterocyclic rings bearing more hetero atoms seemed to be necessary factors in providing higher cytotoxic activities in Raji cell lines.

Acknowledgements. The authors would like to thank the Research Council of Islamic Azad University, Ahvaz Branch for their generous support of this work.

REFERENCES

1. B. Garg and Y.-C. Ling, *Green Mater.*, **2013**, *1*, 47–61.
2. J. T. Robinson, F. K. Perkins, E. S. Snow, Z. Wei and P. E. Sheehan, *Nano Lett.*, **2008**, *8*, 3137–3140.
3. H. Wang, Q. Hao, X. Yang, L. Lu and X. Wang, *Electrochem. Commun*., **2009**, *11*, 1158–1161.
4. L. L. Zhang, X. Zhao, M. D. Stoller, Y. Zhu, H. Ji, S. Murali, Y. Wu, S. Perales, B. Clevenger and R. S. Ruoff, *Nano Lett.*, **2012**, *12*, 1806–1812.
5. A. Dhakshinamoorthy, M. Alvaro, P. Concepcijn, V. Fornus and H. Garcia, *Chem. Commun*., **2012**, *48*, 5443–5445.
6. K. B. Dhopte, D. S. Raut, A. V. Patwardhan and P. R. Nemade, *Synth. Commun*., **2015**, *45*, 778–788.
7. K. B. Dhopte, R. S. Zambare, A. V. Patwardhan and P. R. Nemade, *RSC Adv.*, **2016**, *6*, 8164–8172.
8. S. M. Islam, A. S. Roy, R. C. Dey and S. Paul, J. Mol. Catal. Chem., **2014**, *394*, 66–73.
9. S. Verma, H. P. Mungse, N. Kumar, S. Choudhary, S. L. Jain, B. Sain and O. P. Khatri, *Chem. Commun.*, **2011**, *47*, 12673–12675.
10. M. M. Kadam, O. R. Lokare, K. V. M. K. Kireeti, V. G. Gaikar and N. Jha, *RSC Adv.*, **2014**, *4*, 62737–62745.
11. K. Krishnamoorthy, M. Veerapandian, K. Yun and S.-J. Kim, *Carbon*, **2013**, *53*, 38–49.

12. H. Yan, X. Tao, Z. Yang, K. Li, H. Yang, A. Li and R. Cheng, *J. Hazard. Mater*., **2014**, *268*, 191–198.
13. G. Allaedini, S. M. Tasirin and P. Aminayi, Chem. Pap., **2016**, *70*, 231–242.
14. X. Du, H. Su and X. J. Zhang, *Catal.*, **2020**, *383*, 103–116.
15. M. Ngcobo, G. S. Nyamato and S. O. Ojwach, *Mol. Catal.*, **2019**, *478*, 110590–110596.
16. W. T. Eckenhoff, *Coord. Chem. Rev.*, **2018**, *373*, 295–316.
17. H. Adrienn, H. Zoltán and V. Ilona, *Synth. Commun.*, **2006**, *36*, 129–136.
18. D. Bhattacharjee, D. Sutradhar, A. K. Chandra and B. Myrboh, *Tetrahedron*, **2017**, *73*, 3497–3504.
19. J. Albadi, F. Shirini, B. Ghabezi and T. Seiadatnasab, *Arab. J. Chem.*, **2017**, *10*, S509–S513.
20. A. Ahad and M. Farooqui, *Res. Chem. Intermed.*, **2017**, *43*, 2445–2455.
21. S. R. Cherkupally and R. Mekala, *Chem. Pharm. Bull*., **2008**, *56*, 1002–1004.
22. A. Rahmati and Z. Khalesi, *Tetrahedron*, **2012**, *68*, 8472–8479.
23. Y. B. Xie,S P. Ye, W. F. Chen, Y. L. Hu, D. J. Li and L. Wang, *Asian J. Org. Chem.*, **2017**, *6*, 746–750.
24. S. Dastkhoon, Z. Tavakoli, S. Khodabakhshi, M. Baghernejad and M. K. Abbasabadi, *New J. Chem.*, **2015**, *39*, 7268–7271.
25. A. Khalafi-Nezhad, M. Divar and F. Panahi, *Tetrahedron Lett.*, **2013**, *54*, 220–222.
26. M. Ghashang, S. Jabbarzare, H. Tavakoli, H. Banisadeghi, A. Hosein Sokhanvar, M. Lotfi and A. Chami, *Curr. Nanosci*., **2015**, *11*, 95–100.
27. J. Safari, S. H. Banitaba and S. D. Khalili, *J. Mol. Catal. A Chem.*, **2011**, *335*, 46–50.
28. M. G. Dekamin, E. Kazemi, Z. Karimi, M. Mohammadalipoor and M. R. Naimi-Jamal, *Int. J. Biol. Macromol.*, **2016**, *93*, 767–774.
29. L. Jiang, W. Ye and W. Su, *Chem. Res. Chin. Univ.*, **2019**, *35*, 235–238.
30. A. Maleki, F. Hassanzadeh-Afruzi, Z. Varzi and M. S. Esmaeili, *Mater. Sci. Eng.*, **2020**, *109*, 110502-110508.
31. H. Alinezhad, M. Tarahomi, B. Maleki and A. Amiri, *Appl. Organomet. Chem*, **2019**, *33*, 4661-4668.
32. A. Maleki, R. Firouzi-Haji and Z. Hajizadeh, *Int. J. Biol. Macromol.*, **2018**, *116*, 320–326.
33. R. Taheri-Ledari, J. Rahimi and A. Maleki, *Ultrason. Sonochem.*, **2019**, *59*, 104737–104742.
34. M. G. Sharma, D. P. Rajani and H. M. Patel, *Royal Soc. Open Sci*., **2017**, *4*, 1–8.
35. M. Honari, H. Sanaeishoar, A. R. Kiasat and M. K. Mohammadi, *Res. Chem. Intermediates*, **2021**, *47*, 1829–1841.
36. S. Z. Y. Abadi, M. K. Mohammadi and H. Tavakkoli, *Trends in Pharma. Sci.*, **2021**, *7*, 289–298.
37. J. Azizian, M K. Mohammadi, O. Firuzi, N. Razzaghi-asl and R. Miri, *Med. Chem. Res.*, **2012**, *21*, 3730–3740.
38. L. Xiao, L. Youji, C. Feitai, X. Peng and L. Ming, *RSC Adv.*, **2017**, *7*, 25314–25324.